doi:10.1006/jmbi.2000.4171 available online at http://www.idealibrary.com on IDEAL® J. Mol. Biol. (2000) 303, 667–678

JMB

Molecular-level Thermodynamic and Kinetic Parameters for the Self-assembly of Apoferritin Molecules into Crystals

S.-T. Yau[1], Dimiter N. Petsev[1], Bill R. Thomas[1,2] and Peter G. Vekilov[1]*

[1]*Department of Chemistry University of Alabama in Huntsville, Huntsville AL 35899, USA*

[2]*Universities Space Research Association, Marshal Space Flight Center, Huntsville AL 35875, USA*

**Corresponding author*

The self-assembly of apoferritin molecules into crystals is a suitable model for protein crystallization and aggregation; these processes underlie several biological and biomedical phenomena, as well as for protein and virus self-assembly. We use the atomic force microscope *in situ*, during the crystallization of apoferritin to visualize and quantify at the molecular level the processes responsible for crystal growth. To evaluate the governing thermodynamic parameters, we image the configuration of the incorporation sites, ''kinks'', on the surface of a growing crystal. We show that the kinks are due to thermal fluctuations of the molecules at the crystal-solution interface. This allows evaluation of the free energy of the intermolecular bond $\phi = 3.0\ k_B T = 7.3$ kJ/mol. The crystallization free energy, extracted from the protein solubility, is -42 kJ/mol. Published determinations of the second virial coefficient and the protein solubility between 0 and 40 °C revealed that the enthalpy of crystallization is close to zero. Analyses based on these three values suggest that the main component in the crystallization driving force is the entropy gain of the water molecules bound to the protein molecules in solution and released upon crystallization. Furthermore, monitoring the incorporation of individual molecules in to the kinks, we determine the characteristic frequency of attachment of individual molecules at one set of conditions. This allows a correlation between the mesoscopic kinetic coefficient for growth and the molecular-level thermodynamic and kinetic parameters determined here. We found that step growth velocity, scaled by the molecular size, equals the product of the kink density and attachment frequency, i.e. the latter pair are the molecular-level parameters for self-assembly of the molecules into crystals.

Keywords: ferritin; self-assembly; molecular resolution; interaction energy; solvent entropy

Introduction

Self-assembly of apoferritin molecules into crystals represents a suitable model system for studies of crystallization and related phenomena of biological macromolecules. Despite recent advances in nuclear magnetic resonance techniques (Warren, 1998; Wütrich, 1995), methods based on the diffraction of X-rays, electrons, or neutrons by protein crystals are still widely used for protein structure determinations. Claims that protein crystallization is a major rate-limiting step in structure determinations abound even in recent literature (Chayen *et al.*, 1996; Ducruix & Giege, 1992; McPherson, 1999; Weber, 1997). Beyond protein single crystal growth, progress in various biochemical and biomedical research and production tasks is impeded by the lack of insight into protein nucleation and growth mechanisms. For instance, the slow dissolution rate of protein crystals is used to achieve sustained release of medications, such as insulin and interferon-α (Brange, 1987; Long *et al.*, 1996; Matsuda *et al.*, 1989; Peseta *et al.*, 1989; Reichert *et al.*, 1995). If the administered dose consists of a few, larger, equidimensional crystallites, steady medication release rates can be maintained for longer periods than for doses comprised of many smaller crystallites. Other biomedical applications include pathological conditions related to the for-

E-mail address of the corresponding author: vekilovp@email.uah.edu

0022-2836/00/050667–12 $35.00/0

mation of crystals or less ordered solid aggregates in the human body. Often cited examples are the crystallization of hemoglobin C and the polymerization of hemoglobin S that cause, respectively, the CC and sickle cell diseases (Eaton & Hofrichter, 1990; Hirsch *et al*., 1985). Crystallization of the proteins in the eye lens is associated with the pathology of cataract formation (Berland *et al*., 1992).

The molecules of the chosen model protein, apoferritin are the hollow shells of ferritin, the main non-heme iron storage protein in the cytosol (Harrison & Arosio, 1996; Massover, 1993; Theil, 1987). The molecules have a convenient quasi-spherical shape and in the presence of Cd^{2+} or other divalent metal cations easily form octahedral crystals of the cubic F432 space group with the lattice constant $a = 18.4$ nm. Contrary to typical protein crystallization cases, where the electrolyte serves to screen the repulsion between the similarly charged protein molecules, in the apoferritin case Cd^{2+} is involved in specific bonds between the molecules (Hempstead *et al*., 1997). This specificity makes the case of apoferritin crystallization a relevant first-approximation model of other self-assembling systems: viri, protein complexes, etc. The symmetry of the environment of a molecule in a crystal makes quantitative insight easier to obtain and comprehend.

While crystallization of proteins, as any other material, occurs by the ordered addition of molecules, the resolution of the experimental techniques employed until recently to study these processes was significantly coarser than the molecular sizes (Forsythe *et al*., 1999; Li *et al*., 1999b; Vekilov *et al*., 1998). Only recently images of protein crystal surfaces growing from solution were recorded at molecular (Kuznetsov *et al*., 1999; Rashkovich *et al*., 1998; Yip *et al*., 1998) and even sub-molecular (Malkin *et al*., 1999) resolutions. These studies provided first qualitative data on the molecular structure of the growth steps and of surface point defects.

The coarseness of the applied techniques determined the lack of microscopic data on the processes of molecular self-assembly into aggregates or crystals. Hence, the objective of the investigations reported here was to obtain quantitative molecular-level insight into these processes. The employed method is *in situ* monitoring of the processes of molecular self-assembly with the atomic force microscope (Yau *et al*., 2000; Yau & Vekilov, 2000).

Using this method with the chosen protein system, we first consider the components of the driving force for the processes of aggregation and crystallization. From determinations of the magnitude of the thermal fluctuations of the unfinished layers on the surface of growing crystals (Gibbs, 1961) we aim to extract the free energy of the bond between the protein molecules in the crystal, as done for metals and semiconductors (Kitamura *et al*., 1993; Kuipers *et al*., 1993; Poensgen *et al*., 1992; Swartzentruber, 1998). Using recent data on solubility and the solute interactions obtained as a function of temperature we could distinguish between enthalpy and entropy contributions (Petsev *et al*., 2000a). We will also try to delineate entropy contributions to the crystallization driving force associated with the protein ordering from those due to the changes in the solvent state. Ordering and disordering of the solvent often occurs in processes involving biological macromolecules and may represent a significant fractions of the interaction potential between separate molecules, or between parts of a molecule (Eaton *et al*., 1997; Eisenberg & Crothers, 1979).

Furthermore, we will attempt to determine the molecular-level kinetic constants for binding of solute protein molecules to the growth sites on the crystal surface. By fitting them to independently determined mesoscopic and macroscopic kinetic growth constants, we will test the applicability of the theoretical models for crystallization of biological macromolecules (Chernov & Komatsu, 1995a). More important, such quantitative molecular-level insight has the potential to suggest a rational way of controlling the kinetics of self-assembly by variation of the molecular properties.

Results

Kinks and kink density

Under all conditions used in the experiments reported here, the crystals as seen in the optical microscope attached to the AFM had the typical octahedral shapes with sharp edges. Accordingly, the AFM images in Figure 1 and all Figures below indicate growth by layer generation and spreading to cover the whole facet. This growth mode has been reported for many protein crystals (Durbin & Carlson, 1992; Malkin *et al*., 1996; Yip & Ward, 1996). In a previous AFM study of apoferritin crystallization (Malkin *et al*., 1996), rough interfaces corresponding to the normal growth mode were seen that are typically found on metal and semiconductor crystals growing from the melt (Van der Eerden, 1994). This discrepancy is likely due to either the high protein and precipitant levels used in that earlier study, or to the high impurity content in the commercial apoferritin preparations (Thomas *et al*., 1997) employed by Malkin *et al*. (1996).

The structures of a (111) crystal face and of a growth step are shown in Figure 1. The edges of unfinished layers on the crystal surface are the growth steps. The layers spread by the attachment of molecules to the steps. If we consider a molecule adsorbed on crystal surface away from a step, it is bound to at most three underlying molecules. However, a molecule attached at the step such as one in Figure 1(b) is bound to five molecules (three in the underlying layer and two in the step) belonging to the crystal. Molecules in position 2 in Figure 1(b) are bound to six crystal molecules, i.e. half the number of neighbors that a molecule has

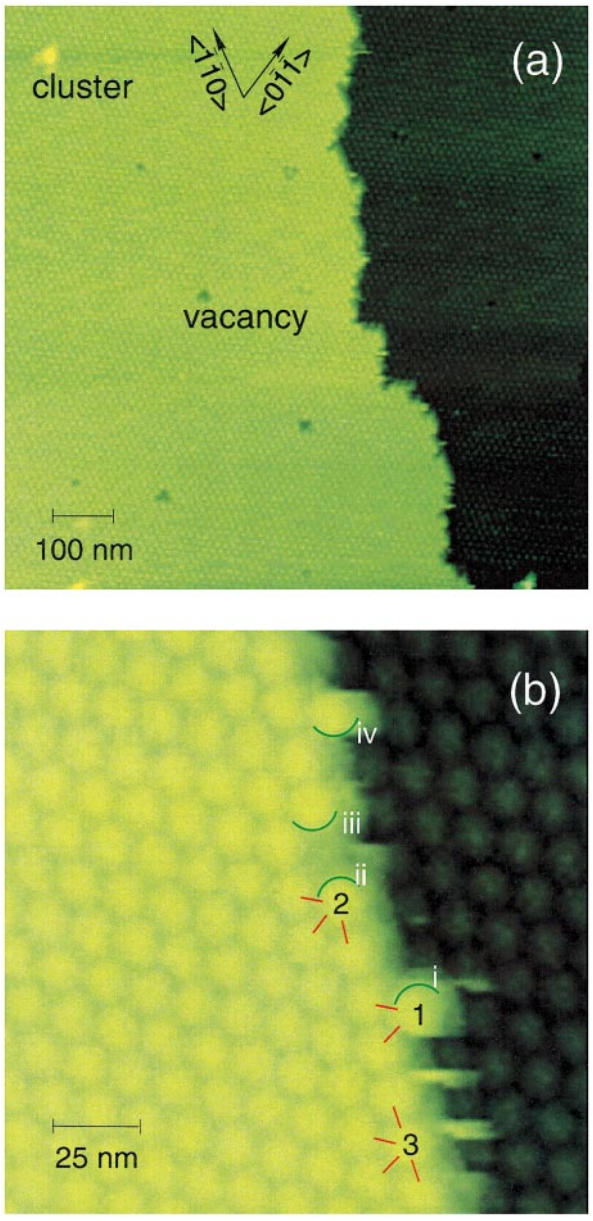

Figure 1. Molecular structures of a growth step on an apoferritin crystal at protein concentration of 70 μg/ml, corresponding to supersaturation $\sigma = 1.1$. Dark green, lower layer; yellow, advancing upper layer. (a) Lower resolution view. Adsorbed impurity clusters and surface vacancies are indicated. (b) Higher resolution view. Three different types of molecular positions at a step are marked with Arabic numbers, for details, see the text. Bonds with molecules belonging to the top crystal layer are marked with red. Green arches and Roman numbers mark potential growth sites, ''kinks''.

in the crystal, while those in position 3-to seven. When a molecule attaches to position 2, the molecular configuration at the step providing six neighbors to an incoming molecule is reproduced and the surface free energy of the crystal is not increased. Hence, it has been postulated that only such locations on the step serve as growth sites (Stranski, 1928; Stranski & Kaischew, 1934; Volmer, 1939). The density of such sites, called ''kinks'', has been introduced as a fundamental variable that determines the ability of the crystal to incorporate solute molecules and grow (Burton, 1951; Chernov, 1984).

From Figure 1 and ~15 other similar images, we determine the kink density along a step by counting the molecules between two kinks, n_k. For instance, in Figure 1(b) n_k between kinks i and ii is three molecules, while between kinks iii and iv is two. The distribution of n_k for the growth conditions in Figure 1 is shown in Figure 2(b). Comparing Figure 2(a), (b) and (c), we see that the n_k distributions are nearly the same near equilibrium, as well as at very high supersaturations, provided that the distance between the steps is higher than ~200 nm.

Figure 3 shows the distribution of n_k along steps spaced about ten molecules (0.13 μm) apart, as opposed to 0.5 to 1 μm in Figures 1 and 2. The kink density and step meandering are lower, indicating interactions between neighboring steps. Such interactions may occur through the solution or through the layer of adsorbed apoferritin molecules on the crystal surface and consist of competition between the steps for nutrient supply. Competition for supply effectively reduces the supersaturation to which a step is exposed. However, the results in Figure 2 indicate that the kink density is independent of the supersaturation within very broad limits. Hence, competition for solute supply is not the interaction underlying the seen decrease in kink density. Other interaction types include step-step repulsion associated with the entropy loss of closely spaced steps (Williams & Bartelt, 1991), or overlapping of the relaxation elastic fields of neighboring step edges (Houssmandzadeh & Misbah, 1995; Marchenko & Parshin, 1980). Our observations are evidence that such interactions may be present even for protein crystal surfaces.

Note that kink density is affected by the presence of surface point defects, such as the vacancies and adsorbed clusters shown in Figure 1(a) (for the identification of those clusters as molecular dimers, see (Petsev *et al.*, 2000b)). These defects act as stoppers: straight step segments as long as eight molecules, similar to those on step 2 in Figure 3(a), form and the step propagation is locally delayed (Yau *et al.*, 2000). For the statistics in Figures 2 and 3(b) we did not consider step segments around such stoppers.

Molecular frequency of attachment to kink sites and kinetics of step propagation

While the kink density is a thermodynamic growth variable that characterizes the affinity of the crystal to the solute molecules, the kinetics of incorporation are reflected by the flux of molecules into a growth site. To monitor these fast incorporation events, we disabled the slow scanning axis of

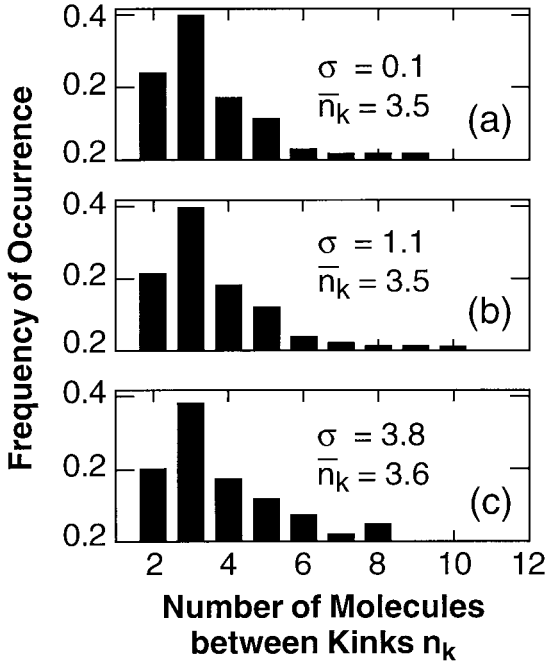

Figure 2. Distribution of number of molecules between kinks on steps located >0.5 μm apart, obtained from images similar to Figure 1 at the three supersaturations σ indicated in the plots, the mean values of the distributions for each case are also shown. The protein concentrations corresponding to these σ's are (a) 25 μg/ml, (b) 70 μg/ml and (c) 1 mg/ml.

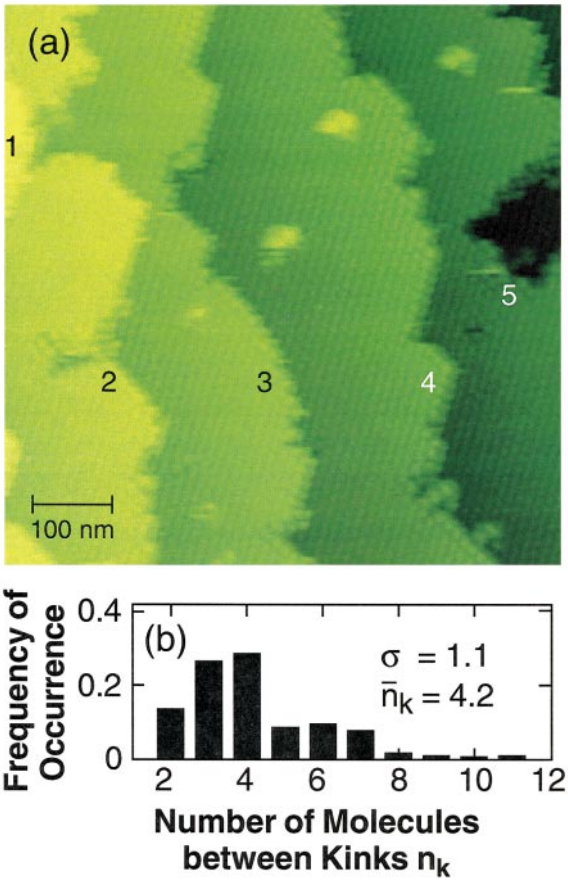

Figure 3. (a) Structure of steps and (b) kink distribution for closely spaced steps at apoferritin concentration of 70 μg/ml, supersaturation $\sigma = 1.1$. Clusters similar to the one in Figure 1 are seen on the terraces behind steps 3, 4, and 5 in (a).

the AFM. The advance of a step site is shown in Figure 4. Figure 5 shows that step motion is not inhibited or accelerated at the location of scanning, i.e. the chosen scanning parameters ensured that step propagation was not affected by scanning over the same line for approximately three minutes.

Despite the relatively high solution supersaturation $\sigma = 1.1$, the time trace in Figure 4 reveals not only 25 arrivals to but also 22 departures of molecules from the monitored site. All arrivals and departures of molecules to and from the monitored site involve single molecules. Therefore, in contrast to claims of preformed multiple-molecule growth units for the protein lysozyme (Li *et al.*, 1999a,b; Nadarajah & Pusey, 1997), apoferritin and ferritin crystal growth by the attachment of single molecules.

This type of data collection does not allow observations of the neighboring sites at the step. We cannot distinguish between attachment/detachment from molecules in the kinks or at the steps. Still, we notice that the residence times τ between these events fall into either $\tau \leqslant 1$ second or $\tau > 5$ seconds. In Figure 4 we have six events of the second type and 19 events of the first. Their ratio is roughly equal to the kink density along the step, suggesting that the long-time events may be attachments/detachments to/from a kink, position 2 in Figure 1(b), while the short ones may be sightings of molecules at the step edge, position 1 in Figure 1(b). Furthermore, molecules may enter the line of observation due either to molecular diffusion along the step or to exchange with either the terrace between the steps or the adjacent solution. While the latter results in step propagation and growth, the former is a process that only involves rearrangement of molecules already belonging to the crystal and may not be associated with growth. In earlier work (Yau *et al.*, 2000), we analyzed the time correlation function of the step position, as done before for steps on metal and semiconductor surfaces (Alfonso, 1992; Bartelt, 1990; Ihle *et al.*, 1998; Kuipers *et al.*, 1993; Poensgen *et al.*, 1992). These analyses indicate that the trace in Figure 4 predominantly reflects exchange of molecules between the step and its environment.

This conclusion allows us to extract from Figure 4 a net frequency of attachment of molecules to kinks. From the net attachment of three molecules for 162 seconds and the probability of viewing a kink of $1/n_k = 1/3.5$, we get

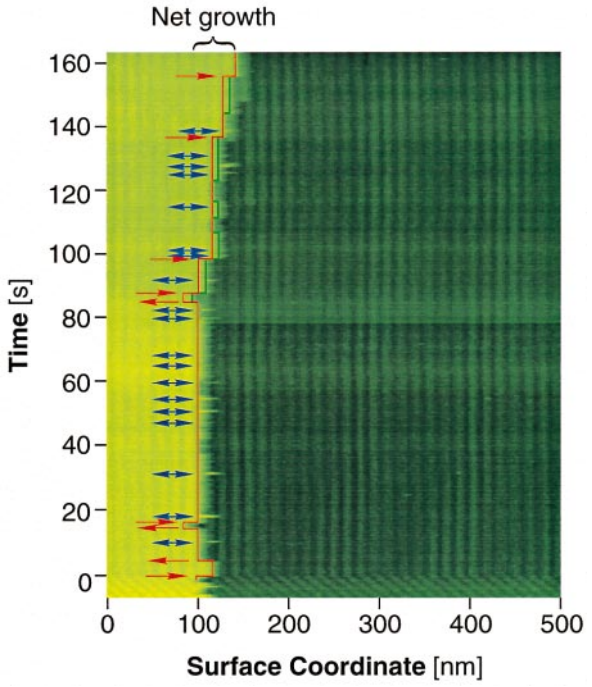

Figure 4. Incorporation of molecules into steps at apoferritin concentration of 70 μg/ml, $\sigma = 1.1$. Pseudo-image recorded using scanning frequency of 3 Hz with the y-scan axis disabled at time =0 shows displacement of one step site. Red contour traces step position. Red arrows indicate attachment and detachment events with residence time >1 second, blue double-sided arrows; with residence time <1 second, for details, see the text. Appearance of 1/2 molecule attachments at times >80 seconds, highlighted in green, is due to events at a neighboring site that enters image due to scanner

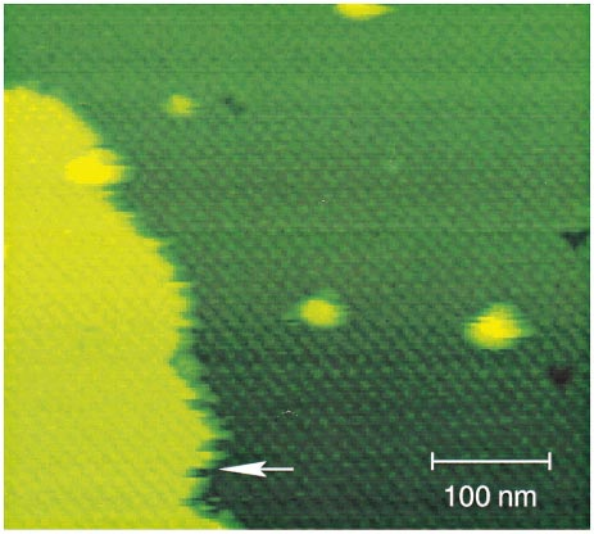

Figure 5. Surface scan immediately after Figure 4, arrow indicates location of monitoring in Figure 4. Clusters and vacancies similar to those in Figure 1 seen on lower terrace.

$f = 0.065\ s^{-1}$, or one molecule per approximately 15 seconds.

The step velocities v averaged over image collection times of approximately 40-50 seconds are shown in Figure 6. The data sets at the first four concentrations fit well the proportionality (Chernov & Komatsu, 1995a,b):

$$v = \beta\Omega C_e(C/C_e - 1) \qquad (1)$$

where $\Omega = 1/4\ a^3 = 1.56 \times 10^{-18}\ cm^3$ is the crystal volume per molecule, C is the apoferritin concentrations and $C_e = 23$ μg/ml (see Materials and Methods) is the concentration at equilibrium between crystal and solution, or the solubility. The averaged step kinetic coefficient, or the macroscopic kinetic constant of growth that emerges from equation (1), is $\beta = 6 \times 10^{-4}$ cm/s. The values of the step velocity v at the highest apoferritin concentration $C = 1$ mg/ml, $C/C_e - 1 = 42$ in Figure 6 are lower by about 30 % from those expected based on the above value of the step kinetic coefficient. The likely reason is the competition for supply between closely spaced steps at the higher step density, as evidenced for other protein systems (Land *et al.*, 1997; Vekilov *et al.*, 1995, 1996).

Discussion

Energy of a kink and the intermolecular bond energy

The lack of dependence of the kink density on the thermodynamic supersaturation suggests that the kinks are not created by nucleation of molecular rows along a step: such nucleation would result in a steep dependence of kink density on supersaturation (Chernov *et al.*, 1999; Teng *et al.*, 1998). Hence, the kink density $1/n_k$ appears to be an equilibrium property of this surface even during growth in a supersaturated environment. In this case, the number of molecules between the kinks n_k is solely determined by the balance of molecular interactions and thermal fluctuations in the top crystal layer (Gibbs, 1961; Kuipers *et al.*, 1993; Swartzentruber, 1998), and should be a function of the energy w needed to create a kink. Derivations have shown (Burton, 1951) that the average $\overline{n}_k$:

$$\bar{n}_k = 1/2 \exp(w/k_B T) + 1 \qquad (2)$$

where T is the absolute temperature and k_B is the Boltzmann constant. From the value of $\overline{n}_k$ in Figure 2, $w = 1.6\ k_B T$. It is quite surprising that this value of w is only slightly lower than the energy of kinks on Si crystals (Swartzentruber *et al.*, 1990): one would expect the strong covalent bonds in the Si crystal lattice to lead to significantly higher kink energies. Quite surprisingly, for the orthorhombic form of lysozyme $w = 7.4\ k_B T$ (Chernov *et al.*, 1999). This significantly higher value leads to an

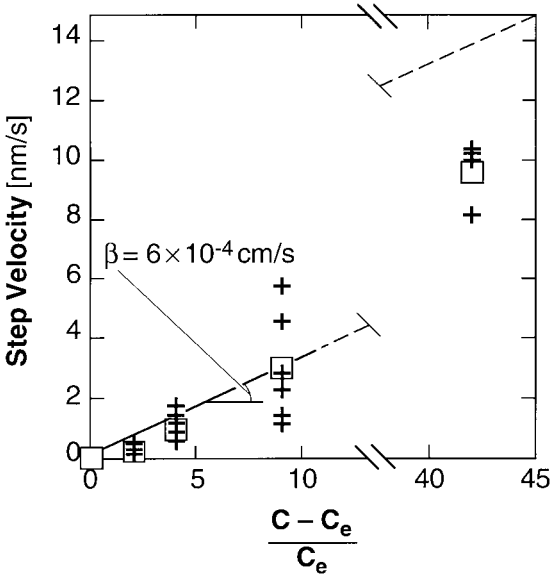

Figure 6. Step velocities v determined by comparing step positions within 44-47 seconds, plotted as function of concentration supersaturation $(C - C_e)\cdot C_e^{-1}$. +, individual determinations: data scatter reflects the stochastic nature of crystal growth at the molecular level; □, average v for each concentration. Continuous line corresponds to shown step kinetic coefficient β.

extremely low kink density with n_k as high as 400-800, and step propagation limited by the rate of kink generation (Chernov *et al.*, 1999).

If we assume first-neighbor interactions only, we can evaluate the intermolecular bond energy, ϕ. When a molecule is moved from within the step on a (111) face of a face centered cubic (fcc) crystal (position 3 in Figure 1(b)) to a location at the step (position 1 in Figure 1(b)), four kinks are created. For this, seven bonds (four in the top layer and three with molecules from the underlying layer) are broken, and five are formed. Then, $w = \phi/2$ and $\phi = 3.2\ k_BT \cong 7.8$ kJ/mol.

The intermolecular bonds in ferritin and apoferritin crystals involve two chains of bonds Asp-Cd^{2+}-Glu between each pair of adjacent molecules (Hempstead *et al.*, 1997; Lawson *et al.*, 1991). The above value of ϕ seems significantly lower than the typical coordination bond energies. This low value may stem from the need to balance Cd^{2+} coordination with the aminoacid residues and with the water species (H_2O and OH^-), or from spatial constrains imposed by the other aminoacid residues involved in the intermolecular contacts.

Second and third neighbor effects

Some of the protein-protein molecular interactions, such as the electrostatic, may have range longer than the diameter of one molecule (Beresford-Smith *et al.*, 1985). Then, interactions with second and third neighbors will contribute to the interactions of a molecule with a site on the crystal surface. This will affect the dynamics of the kinks and bias the determination of the intermolecular bond energy from kink density measurements.

To account for possible second and third neighbor effects in the crystal as well as in the evolving molecular row, we carried out model calculations. We considered an ordered layer of spherical molecules deposited on a octahedral face of a fcc crystal. As in many previous works with proteins (Sear, 1999; ten Wolde & Frenkel, 1997), we approximate the interaction energy between the molecules with a Lennard-Jones type potential. Then, the energy of interaction of a molecule with another molecule labeled i at a distance r_i will be:

$$U_i = \varepsilon\left[\left(\frac{r^*}{r_i}\right)^{12} - 2\left(\frac{r^*}{r_i}\right)^{6}\right] \qquad (3)$$

Here, ε is the depth of the potential well and r^*, the position of the minimum, is chosen as the crystallographic distance between the molecules, 13 nm. The function $U_i(r_i/r^*)$ is plotted in Figure 7(b). Furthermore, we assume that the total ''potential'' energy of a molecule can be calculated as superposition of the pair interactions with all other molecules in the of equation (3). In this way, all molecules in the crystal will be in the energy minima of their interactions with the other molecules in the crystal. Note that unlike (Hagen & Frenkel, 1994; ten Wolde & Frenkel, 1997), we take the position of the minimum r^* from the experimental data and do not optimize the crystal structure.

We are only interested in the dynamics of kinks at a step. Hence, the energy of interaction with the molecules of the substrate provides a constant additive to the energy of the molecules under consideration and we can limit the calculations to the top layer. Furthermore, we found that the contribution of all neighbors beyond the second shell is negligible. As a result, in the calculations we account for up to fourth neighbors. This allows us to limit the modeled layer to an island of 4×10 molecules. Choosing $\varepsilon = 3\ k_BT$, we get the potential relief of the interaction of a molecule with this island shown as 1 in Figure 7(a).

To simulate the formation of kinks, we remove a molecule from the edge of the island, forming two kinks, and calculate the new energy relief. The energy spent for this removal is equal to the deepest minimum in 2 in Figure 7(a). Another mechanism of kink fomation is by the attachment of molecules to the step to form configuration 3. The corresponding energy gain is equal to the depth of the wells near the middle of the long island edge in 1. The net sum of the gain and the loss, needed to calculate the average energy to form a kink is $= 6.2\ k_BT$.

As a next step, we remove a molecule next to the vacancy in 2 to obtain the configuration 4 and deposit a molecule in the minimum above the

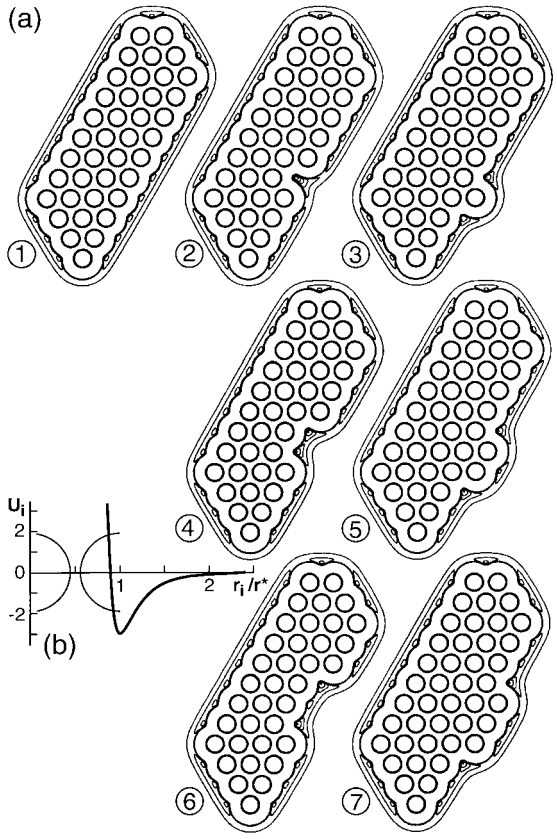

Figure 7. Model results. (a) Contour plot of the potential energy U of a single molecule in the vicinity of an island deposited on an octahedral face of a face-centered cubic crystal. ΔU between two contours is k_BT. Individual molecules belonging to the island represented by circles; the appearance of a thick line that follows the contour of the island is a result of steep gradient of U between the minimum and the molecules. (b) Plot of equation (3) with U_i in k_BT units; arches indicate surfaces of adjacent molecules.

molecule attached at the edge in 3 producing the configuration 5. The net loss from these two operations equals the difference between the top minimum in the vacancy in 4 and at the used site in 3. We get 0.2 k_BT. Then we remove a molecule next to the double vacancy in 4 to produce 6 and attach it in line with the previous two molecules at the island periphery in 5 to produce 7. The net contribution of this operation, calculated in the same fashion as the others, is negligible. It is not surprising that we found same result for removing a fourth molecule from the vacancy cluster in 6 and adding it to the line of attached molecules in 7.

Summing the total energy expenditure, we get 6.4 k_BT as the energy needed to generate four kinks. The average energy for formation of one kink w is 1.6 k_BT, adjusted to the experimentally found value by selecting the appropriate ε. If we assume that the depth of the Lenard-Jones well ε is a good equivalent to the intermolecular bond energy ϕ, we see that accounting for higher neighbor effects, at least in the first approximation used here, decreases this value from 3.2 to 3 k_BT, i.e. by ~7 %.

Enthalpy, entropy and free energy for crystallization

The intermolecular bond energy ϕ contains both enthalpy and entropy components. The enthalpy ones are due to the ion-mediated, hydrogen, and other bonds between the molecules, while the entropy components stem from the net release or binding of water and other small molecules upon crystallization (Eisenberg & Crothers, 1979, p. 164). With this in mind, we can write an expression for the free energy for crystallization as:

$$\Delta G^\circ = \Delta H^\circ_{\text{bond}} - T\Delta S^\circ_{\text{bond}} - T\Delta S^\circ_{\text{protein}} \qquad (4)$$

Here $\Delta H^\circ_{\text{bond}} - T\Delta S^\circ_{\text{bond}}$ are contributions associated with ϕ, and $\Delta S^\circ_{\text{protein}}$ is the loss of entropy of the protein molecules. A crude estimate of $\Delta S^\circ_{\text{protein}}$ and of the relative weights of the two entropy contributions can be obtained by comparing the standard free energy change for apoferritin crystallization ΔG° determined from the solubility, to the value corresponding to the intermolecular bond free energy ϕ.

The calculate ΔG°, we convert the solubility of the apoferritin at the chosen crystallization conditions 23 μg/ml, see Methods below, to molar concentration $C_e = 5.2 \times 10^{-8}$ M. At equilibrium between crystal and solution, for the apoferritin:

$$\Delta G = G^\circ(\text{crystal}) - [G^\circ(\text{solution}) + N_A k_B T \ln(\gamma C_e)] = 0 \qquad (5)$$

where N_A is the Avogadro number, γ is the protein activity coefficient, and the product $N_A k_B = R$ is the universal gas constant (Atkins, 1998). Hence:

$$\Delta G^\circ = G^\circ(\text{crystal}) - G^\circ(\text{solution}) = N_A k_B T \ln(\gamma C_e) \qquad (6)$$

(Eisenberg & Crothers, 1979). Using $\gamma \cong 1$ for solutions in which the attraction and repulsion between the molecules are practically balanced, see METHODS below, $\Delta G^\circ = -42$ kJ/mol.

To get $\Delta H^\circ_{\text{bond}} - T\Delta S^\circ_{\text{bond}}$ from $\phi = 3$ $k_BT \cong 7.3$ kJ/mol, we have to multiply ϕ by $Z_1/2 = 6$, the half number of neighbors in the crystal lattice (two molecules partake in a bond, in a fcc lattice $Z_1 = 12$) and, accounting for the sign, we get −44 kJ/mol. The closeness of $\Delta H^\circ_{\text{bond}} - T\Delta S^\circ_{\text{bond}}$ to ΔG° indicates the insignificance of $\Delta S^\circ_{\text{protein}}$ for the free energy of crystallization. This insignificance may stem from the huge number ($10^3 - 10^4$) of water molecules that may be associated to a single apoferritin molecule in the solution. In this respect, the investigated protein solution system appears similar to colloid systems, in which the ratio between the numbers of the colloid particles and the solvent molecules is often

similar and ΔS° due to the aggregation of colloid particles is low (Poon *et al.*, 1996).

To evaluate ΔH°_{bond} we used data on the temperature dependencies of the protein solubility and of the second virial coefficient in the range from 0 to 40 °C (Petsev *et al.*, 2000a). According to the results of that study, neither of solubility, not the second virial coefficient has noticeable dependence on temperature. Therefore, the enthalpy of crystallization and the related energy of pair interactions in the solution are close to zero. In combination with the insignificance of $\Delta S^{\circ}_{protein}$, this allows us to conclude that crystallization is mostly driven by the maximization of the entropy of the solvent. Such disordering may stem from a significant disordering of the water and other solvent components bound to the protein molecules in the solution. A similarity can be traced to the processes that underlie hydrophobic attraction that governs many processes in nature (Israelachvili, 1995), including some stages of protein folding (Eaton *et al.*, 1997).

Molecular-level parameters underlying the macroscopic growth kinetics

The results on the incorporation of molecules into a growth site in Figure 4 indicate that, even at the relatively high $\sigma = 1.1$, incorporation of molecules into the crystal is extremely slow and occurs at macroscopic time scales. Furthermore, the ratio of 25 arrivals and 22 departures, mostly due to exchange with the medium, indicates that crystal growth is a very selective process even at such high supersaturations. If foreign or misoriented molecules attach to a step, they have significant chances of detaching into the solution and freeing the space for a proper molecular attachment. This may underlie the purification upon crystallization, utilized in various technological processes.

The step kinetic coefficient β, extracted from the step velocity data averaged over 40-50 seconds in Figure 6 is $\beta = 6 \times 10^{-4}$ cm/s. This value is comparable to values of other, faster growing proteins, indicating that the low net flux and step velocities of this protein are caused by the low solution concentration, reflected in the molecular density ratio between the solution and crystal, $\Omega C_e = 5 \times 10^{-5}$. For comparison, the value of ΩC_e for a another well studied protein, lysozyme growing from a 50 mg/ml solution is as high as 0.02 (Vekilov & Rosenberger, 1996).

The determinations of the step velocities and corresponding kinetic coefficient allows a test of the molecular mechanism of incorporation into steps underlying step motion and the definition of β (Chernov, 1989; Chernov & Komatsu, 1995b). According to these works, the step velocity v:

$$v = a(1/\bar{n}_k)f \qquad (7)$$

where a is the molecular diameter, $1/\bar{n}_k$ is the kink density and f is the frequency of molecular incorporation into kinks. Using the respective values $a = 13$ nm, $\bar{n}_k = 3.5$ and $f = 0.065$ s^{-1} from Figures 2, 4, and 8 we get $a(1/\bar{n}_k)f = 0.24$ nm/s. At the conditions corresponding to those for Figure 4, $(C/C_e - 1) = 2$, $\sigma = 1.1$, the average step velocity from Figure 6 is $v = 0.26$ nm/s. The nearness of the predicted and actual values indicates that kink density and net frequency of attachment to a kink are the fundamental molecular level variables that fully determine the rate of step propagation during crystal growth.

Materials and Methods

Solution preparation

Apoferritin stock solutions were separated into Monomer, Dimer and ''Trimer'' fractions as described in detail elsewhere (Petsev *et al.*, 2000b; Thomas *et al.*, 1997). All experiments discussed here were carried out using the Monomer fraction. The sum residual amount of Dimer and ''Trimers'' in this fraction after purification was ~5 % (w/w). To induce crystallization, $CdSO_4$ was added to concentration in the crystallizing solution of 2.5 % (w/v).

Crystallization and atomic force microscopy imaging

Droplets of crystallizing solution of ~50 μl were placed on 12 mm glass coverslips mounted on iron disks. To avoid evaporation, the droplets were covered with glass covers, hermetically sealed and left overnight in a controlled temperature room at ~22 °C. Typically, this lead to the formation of three to 20 crystals of sizes ranging from 20 to 200 μm firmly attached to the glass bottom. Droplets with three to five crystals were selected and magnetically mounted on the AFM scanner. The fluid AFM cell was filled with crystallizing solution and imaging commenced.

Temperature in the laboratory was stabilized to ~22 °C. No additional temperature control of the solution in the AFM fluid cell was employed. Tests by inserting a thermocouple in the crystallizing solution revealed that its temperature was higher by ~0.5-1.0 deg.C than the room temperature. The documented insensitivity of apoferritin crystallization to temperature variations (Petsev *et al.*, 2000a) justifies this approach to temperature control.

All images were collected *in situ* during the growth of the crystals using the less intrusive tapping imaging mode (Hansm *et al.*, 1994; Noy *et al.*, 1998). This allows visualization of adsorbed protein and impurity species (tip impact in contact imaging mode often prevents such imaging). We also employed scans with disabled *y*-axis, similar to previous STM work on metals and semiconductors in ultra-high vacuum by (Giesen-Seibert *et al.*, 1993; Kitamura *et al.*, 1993; Poensgen *et al.*, 1992). The technique allows monitoring of processes with characteristic times of fractions of a second.

We used the standard SiN tips and tapping drive frequency was adjusted in the range 25-31 kHz to the resonance value for specific tip used. Other scanning parameters were adjusted such that continuous imaging affected neither the surface structure, nor the process dynamics. For verification, we varied the scan sizes and the time elapsed between image collections, and saw

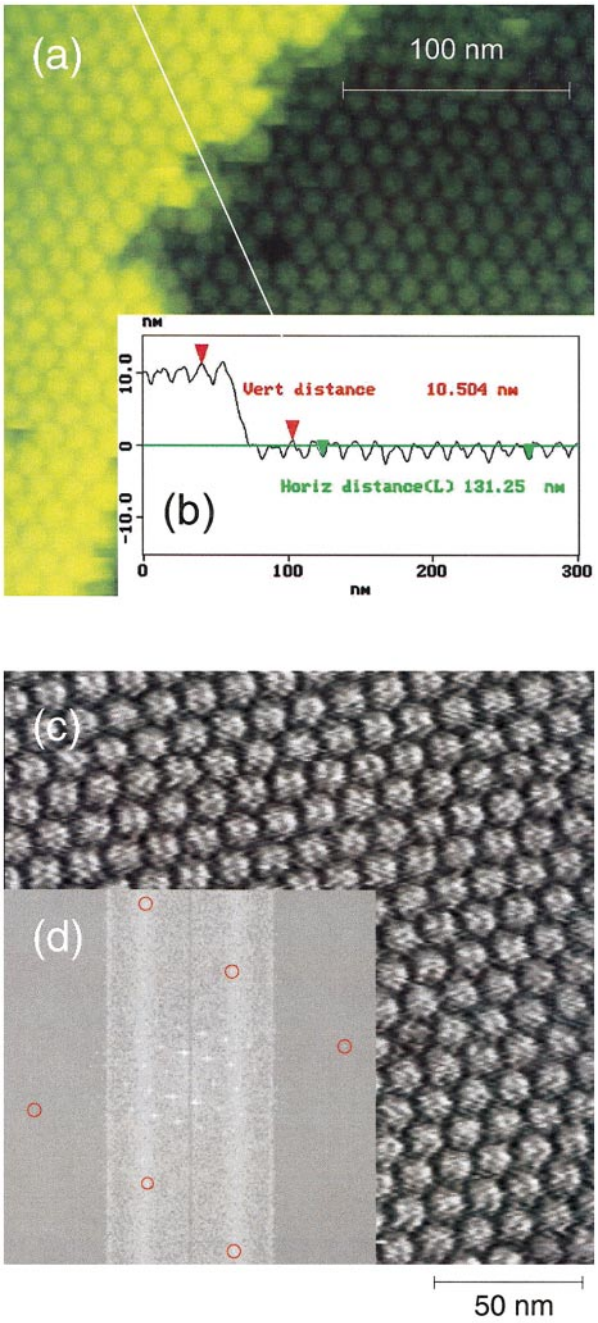

Figure 8. Accuracy and resolution of atomic force microscopy imaging. (a) View of [111] apoferritin crystal face. (b) Height profile along line in (a) allowing determination of layer thickness and molecular spacing. (c) Determination of the resolution limits of the atomic force microscopy imaging used in these studies. Real space high-resolution image (d) Fourier transform of (c), red circles highlight high-resolution peaks; 8th order peaks at top and bottom of image correspond to resolution of ~1.6 nm.

that neither the spatial nor the temporal characteristics of the processes changed.

To test the accuracy of the determination of lateral and vertical dimensions by the AFM, we determined the periodicity within the molecular rows along the {110} directions and the thickness of the [111] layers. Figure 8(a) and (b) and similar analysis of many other images yield values for these two quantities of 13 and 10.5 nm, respectively. These dimensions agree well with calculations, based on the F432 crystal structure. The crystal lattice parameter is $a = 18.4$ nm (Hempstead *et al.*, 1997; Lawson *et al.*, 1991). Therefore, the distance between centers of molecules along the {110} directions is $(1/2)\cdot(2a^2)^{1/2} = 13.0$ nm and the distance between [111] layers is $(1/3)\cdot(3a^2)^{1/2} = 10.6$ nm.

To evaluate the lateral resolution limit of our AFM imaging technique, we scanned a 200 nm × 200 nm square on the surface of a ferritin crystal without steps. The individual molecules in Figure 8(c) are readily distinguishable and some sub-molecular details are detectable. To quantify the resolution of the imaging, we computed the two-dimensional Fourier transform of this image, using the respective module from the Nanoscope IIIa software package. The Fourier image has the expected hexagonal symmetry, with the distance between the peaks in the first hexagon and the center of the plot corresponding to resolution equal to the molecular size of 13 mn. The maximum resolution, determined from the location of the most distant peak in Figure 8(d), is 1.6 nm. Similar analyses with other images of comparable size revealed that typically the resolution was between 5 and 2.5 nm.

The molecular details in Figure 8(c) do not seem to possess translational symmetry. Careful observation allows identification of several sets of molecules with similar features that are randomly distributed throughout the image. The general impression is that the molecules on the surface have several rotational orientations, different from the crystallographically required orientation on a (111) face. We tentatively relate this apparent absence of translational crystallographic symmetry with the lack of consistent decoration pattern of the molecules on surfaces frozen-hydrated ferritin crystals examined by electron microscopy (S. Weinkauf, personal communication). Such patterns have been obtained with crystals of a number of other proteins and protein complexes (Bacher *et al.*, 1992; Meining *et al.*, 1995; Weinkauf *et al.*, 1991).

Note that crystals grown under conditions identical to those used in these studies diffract X-rays and the resolution limit is 1.8-1.85 Å (Thomas *et al.*, 1997). Therefore, it is unlikely that any molecular rotational disorder is present in the crystal bulk. Assuming that Figure 8(c) suggests such disorder in the surface layer of the crystal, the mechanism by which these molecules reorient as the crystal grows poses an intriguing problem.

The lack of translational symmetry of the submolecular details in Figure 8(c) indicates that some of the finer features of the molecules seen in Figure 8(c) will not be reflected by the Fourier transform in Figure 8(d). Hence, the resolution of the AFM imaging may be higher than the values suggested by Figure 8(d).

Solubility and driving force for crystallization

To determine the solubility of the apoferritin at the chosen temperature, pH and buffer and precipitant concentrations, we monitored trains of growth steps and gradually decreased the apoferritin concentration in the solution. We found that at $C = 23$ μg/ml, the propagation of the steps stops, and when the concentration is lower below this value, the step movement was back-

wards and the crystal was dissolving. Repetitions of this procedure allowed determination of the range of this measurement, $C_e = 23(\pm 5)\ \mu g/cm^3$.

Supersaturation σ in protein crystallization studies has often been defined as $\sigma = \ln(C/C_e)$ and this σ has been taken as a measure of the chemical potential difference between solution and crystal $\Delta\mu$ in k_BT units. Such assumption implies solution ideality. To evaluate the non-ideality of the crystallizing solutions, we employed static and dynamic light scattering as described by Petsev *et al*. (2000b). The found value of the second virial coefficient $B_2 = -2.35 \times 10^{-5}\ cm^3\ mol/g^2$.

Following the logic of (Guo *et al*., 1999), it is easy to show that non-ideality leads to a correction in the above expression for the supersaturation:

$$(\mu_{cr} - \mu_p)/k_BT = \Delta\mu/k_BT = \ln(C/C_e) + 2B_2M(C - C_e) + \cdots \quad (8)$$

where $M = 440{,}000$ Da is the protein molecular mass.

Using the above value of B_2 the correction $2\ B_2M(C - C_e) = -0.03$, i.e. $\sim -0.8\,\%$ of $\ln(C/C_e) = 3.77$ at $C = 1$ mg/ml, the highest protein concentration employed in the experiments. Hence the use of the simplified definition of $\sigma = \Delta\mu/k_BT = \ln(C/C_e)$ is justified in this case.

For other proteins under crystallizing conditions, the values of B_2 are limited from below to $\sim -8 \times 10^{-4}\ cm^3\ mol/g^2$ (George & Wilson, 1994; Guo *et al*., 1999; Rosenbaum & Zukoski, 1996). At higher concentrations of proteins of higher molecular masses, the non-ideality correction may lead to a supersaturation significantly smaller than what the simplified definition may suggest.

Acknowledgments

We thank C. Kundrot, S. Weinkauf, A. McPherson and M. Machius for discussions and helpful suggestions on some aspects of this work, O. Galkin for critical reading of the manuscript, and L Carver for expert graphics work. This research was supported by NHLBI, NIH (Grant No HL58038), NASA (Grants No NAG8-1354 and 97 HEDS-02-50), and the State of Alabama through the Center for Microgravity and Materials Research at the University of Alabama in Huntsville.

References

Alfonso, C., Bermond, J. M., Heyraud, J. C. & Metois, J. J. (1992). The meandering of steps and the terrace width distribution on clean Si(111). *Surf. Sci.* **262**, 371-381.

Atkins, P. (1998). *Physical Chemistry*, sixth edit., Freeman, New York.

Bacher, A., Weinkauf, S., Bachmann, L., Ritsert, K., Baumeister, W., Huber, R. & Ladenstein, R. (1992). Electron microscopy of decorated crystals for the determination of the crystallographic rotation and translation parameters in large protein complexes. *J. Mol. Biol.* **225**, 1065-1073.

Bartelt, N. C., Einstain, T. L. & Williams, E. D. (1990). The influence of step-step interactions on step wandering. *Surf. Sci. Letters,* **240**, L591-L598.

Beresford-Smith, B., Chan, D. Y. C. & Mitchell, D. J. (1985). The electrostatic interaction in colloidal systems with low added electrolyte. *J. Colloid Interface Sci.* **105**, 216-235.

Berland, C. R., Thurston, G. M., Kondo, M., Broide, M. L., Pande, J., Ogun, O. & Benedek, G. B. (1992). Solid-liquid phase boundaries of lens protein solutions. *Proc. Natl Acad. Sci. USA,* **89**, 1214-1218.

Brange, J. (1987). *Galenics of Insulin*, Springer, Berlin.

Burton, W. K., Cabrera, N. & Frank, F. C. (1951). The growth of crystals and equilibrium structure of their surfaces. *Phil. Trans. Roy. Soc. London Ser. A,* **243**, 299-360.

Chayen, N. E., Boggon, T. J., Casseta, A., Deacon, A., Gleichmann, T. & Habash, J., *et al*. (1996). Trends and challenges in experimental macromolecular crystallography. *Quart. Rev. Biophy.* **29**, 227-278.

Chernov, A. A. (1984). *Modern Crystallography III: Growth of Crystals*, Springer, Berlin.

Chernov, A. A. (1989). Growth of crystals from solutions. *Contemp. Phys.* **30**, 251-276.

Chernov, A. A. & Komatsu, H. (1995a). Principles of crystal growth m protein crystallization. In *Science and Technology of Crystal Growth* (van der Eerden, J. P. & Bruinsma, O. S. L., eds), pp. 329-353, Kluwer Academic, Dordrecht.

Chernov, A. A. & Komatsu, H. (1995b). Topics in crystal Growth Kinetics. In *Science and Technology of Crystal Growth* (van der Eerden, J. P. & Bruinsma, O. S. L., eds), pp. 67-80, Kluwer Academic, Dordrecht.

Chernov, A. A., Rashkovich, L. N., Yamlinski, I. V. & Gvozdev, N. V. (1999). Kink kinetics, exchange fluxes, 1D ''nucleation'' and adsorption on the (010) face of orthorhombic lysozyme crystals. *J. Phys. Condens. Matter,* **11**, 9969-9984.

Ducruix, A. & Giege, R. (1992). *Crystallization of Nucleaic Acids and Proteins. A Practical Approach*, IRL Press, Oxford.

Durbin, S. D. & Carlson, W. E. (1992). Lysozyme crystal growth studied by atomic force microscopy. *J. Crystal Growth,* **122**, 71-79.

Eaton, W. A. & Hofrichter, J. (1990). Sickle cell hemoglobin polimerization. In *Advances in Protein Chemistry* (Anfinsen, C. B., Edsal, J. T., Richards, F. M. & Eisenberg, D. S., eds), vol. 40, pp. 63-279, Academic Press, San Diego.

Eaton, W. A., Munoz, V., Thompson, P. A., Chan, C. K. & Hofrichter, J. (1997). Submillisecond kinetics of protein folding. *Curr. Opin. Struct. Biol.* **7**, 10-14.

Eisenberg, D. & Crothers, D. (1979). *Physical Chemystry with Applications to Life Sciences*, The Benjamin/Cummins, Menlo Park.

Forsythe, E. L., Nadarajah, A. & Pusey, M. L. (1999). Growth of (101) faces of tetragonal lysozyme crystals: measured growth-rate trends. *Acta Crystallog. sect. D,* **55**, 1005.

George, A. & Wilson, W. W. (1994). Predicting protein crystallization form a dilute solution property. *Acta Crystallog. sect. D,* **50**, 361-365.

Gibbs, J. W. (1961). *The Collected Works of J. W. Gibbs,* 1, Yale University Press, New Haven.

Giesen-Seibert, M., Jentjens, R., Poensgen, M. & Ibach, H. (1993). Time dependence of step fluctuations on vicinal copper (1119) surfaces investigated by tunneling microscopy. *Phys. Rev. Letters,* **71**, 3521-3524.

Guo, B., Kao, S., McDonald, H., Wilson, W. W., Asanov, A. & Combs, L. L. (1999). Correlation of second virial coefficients and solubilities useful in protein crystal growth. *J. Crystal Growth,* **196**, 424-433.

Hagen, M. H. J. & Frenkel, D. (1994). Determination of phase diagrams for the hardcorte attractive Yukawa systems. *J. Chem. Phys.* **101**, 4093-4097.

Hansma, P. K., Cleveland, J. P., Radmacher, M., Walters, D. A., Hillner, P. & Bezanilla, M., *et al*. (1994). Tapping mode atomic force microscopy in liquids. *Appl. Phys. Letters,* **64**, 1738-1740.

Harrison, P. M. & Arosio, P. (1996). The ferritins: molecular properties, iron storage function and cellular regulation. *Biochim. Biophys. Acta,* **1275**, 161-203.

Hempstead, P. D., Yewdall, S. J., Fernie, A. R., Lawson, D. M., Artymiuk, P. J. & Rice, D. W., *et al*. (1997). Comparison of the three dimensional structures of recombinant human H and horse L ferritins at high resolution. *J. Mol. Biol.* **268**, 424-448.

Hirsch, R. E., Raventos-Suarez, C., Olson, J. A. & Nagel, R. L. (1985). Ligand state of intraerythrocytic circulating HbC crystals in homozygote CC patients. *Blood,* **66**, 775-778.

Houssmandzadeh, B. & Misbah, C. (1995). Elastic interaction between modulated steps on a vicinal surface. *J. Phys. I France,* **5**, 685-698.

Ihle, T., Misbah, C. & Pierre-Louis, O. (1998). Equilibrium step dynamics of vicinal surfaces revisited. *Phys. Rev. B,* **58**, 2289-2309.

Israelachvili, J. N. (1995). *Intermolecular and Surface Forces*, Academic Press, New York.

Kitamura, N., Lagally, M. G. & Webb, M. B. (1993). Real-time observations of vacancy diffsuoion on Si(001)-(2x2) by scanning tuneling microscopy. *Phys. Rev. Letters,* **71**, 2081-2085.

Kuipers, L., Hoogeman, M. & Frenken, J. (1993). Step dynamics on Au(110) studied with a high-temperature, high-speed scanning tunneling microscope. *Phys. Rev. Letters,* **71**, 3517-3520.

Kuznetsov, Y. G., Konnert, J., Malkin, A. J. & McPherson, A. (1999). The advancement and structure of growth steps on thaumatin crystals visualized by atomic force microscopy at molecular resolution. *Surf. Sci.* **440**, 69-80.

Land, T. A., DeYoreo, J. J. & Lee, J. D. (1997). An *in situ* AFM investigation of canavalin crystallization kinetics. *Surf. Sci.* **384**, 136-155.

Lawson, D. M., Artymiuk, P. J., Yewdall, S. J., Smith, J. M. A., Livingstone, J. C. & Trefry, A., *et al*. (1991). Solving the structure of human H ferritin by genetically engineering intermolecular crystal contacts. *Nature,* **349**, 541-544.

Li, M., Nadarajah, A. & Pusey, M. L. (1999a). Determining the molecular-growth mechanisms of protein crystal faces by atomic force microscopy. *Acta Crystallog. sect. D,* **55**, 1036.

Li, M., Nadarajah, A. & Pusey, M. L. (1999b). Growth of (101) faces of tetragonal lysozyme crystals: determination of the growth mechanism. *Acta Crystallog. sect. D,* **55**, 1012.

Long, M. L., Bishop, J. B., Nagabhushan, T. L., Reichert, P., Smith, G. D. & DeLucas, L. J. (1996). Protein crystal growth in microgravity review of large scale temperature induction method. *J. Crystallog. Growth,* **168**, 233-243.

Malkin, A. J., Kuznetsov, Y. G., Glanz, W. & McPherson, A. (1996). Atomic force microscopy studies of surface morphology and growth kinetics of thaumatin crystallization. *J. Phys. Chem.* **100**, 11736-11743.

Malkin, A. J., Kuznetsov, Y. G., Lucas, R. W. & McPherson, A. (1999). Surface processes in the crystallization of turnip yellow mosaic virus visualized by atomic force microcsopy. *J. Struct. Biol.* **127**, 35-43.

Marchenko, V. I. & Parshin, A. Y. (1980). Elastic properties of crystal surfaces. *Sov. Phys. JETP,* **52**, 129-131.

Massover, W. H. (1993). Ultrastructure of ferritin and apoferritin: a review. *Micron,* **24**, 389-437.

Matsuda, S., Senda, T., Itoh, S., Kawano, G., Mizuno, H. & Mitsui, Y. (1989). New crystal form of recombinant murine interferon-β. *J. Biol. Chem.* **264**, 13381-13382.

McPherson, A. (1999). *Crystallization of Biological Macromolecules*, Cold Spring Harbor Laboratory Press, Cold Spring Harbor, NY.

Meining, W., Bacher, A., Bachmann, L., Schmid, C., Weinkauf, S., Huber, R. & Nar, H. (1995). Elucidation of the crystal packing by X-ray diffraction and freeze etching electron microscopy. Studies on GTP cyclohydrolase I of *Escherichia coli*. *J. Mol. Biol.* **253**, 208-218.

Nadarajah, A. & Pusey, M. L. (1997). Growth mechanism of the (110) face of tetragonal lysozyme crystals. *Acta Crystallog. sect. D,* **53**, 524.

Noy, A., Sanders, C. H., Vezenov, D. V., Wong, S. S. & Lieber, C. M. (1998). Chemically sensitive imaging in tapping mode by chemical force microscopy: relationship between phase lag and adhesion. *Langmuir,* **14**, 1508-1511.

Peseta, S., Langer, J. A., Zoon, K. C. & Samuel, C. E. (1989). Interferons and their actions. In *Annual Review of Biochemistry* (Richardson, C. C., Boyer, P. D., Dawid, I. B. & Meister, A., eds), vol. 56, pp. 727-778, Annual Reviews, Palo Alto.

Petsev, D. N., Thomas, B. R., Yau, S.-T., Tsekova, D., Nanev, C., Wilson, W. W. & Vekilov, P. G. (2000a). Temperature-independent solubility and interactions between apoferritin monomers and dimers in solution. *J. Crystal Growth,* **In the press**.

Petsev, D. N., Thomas, B. R., Yau, S.-T. & Vekilov, P. G. (2000b). Interactions and aggregation of apoferritin molecules in solution: effects of added electrolytes. *Biophyiscal J.* **78**, 2060-2069.

Poensgen, M., Wolf, J., Frohn, J., Giesen, M. & Ibach, H. (1992). Step dynamics on Ag(111) and Cu(100) surfaces. *Surf. Sci.* **274**, 430-440.

Poon, W., Pusey, P. & Lekkerkerker, H. (1996). Colloids in suspense. *Phys. World,* 27-32.

Rashkovich, L. N., Gvozdev, N. V. & Yamlinski, I. V. (1998). The mechanism of step motion in growth of lysozyme crystals. *Crystallog. Reports,* **43**, 669-697.

Reichert, P., McNemar, C., Nagabhushan, N., Nagabhushan, T. L., Tindal, S. & Hruza, A. (1995). Metal-interferon-alpha crystals. In US Patent, 5,441,734.

Rosenbaum, D. & Zukoski, C. F. (1996). Phase behavior of small attractive colloid particles. *Phys. Rev. Letters,* **76**, 150-153.

Sear, R. P. (1999). Phase behaviour of a simple model of globular proteins. *J. Chem. Phys.* **111**, 4800-4806.

Stranski, I. N. (1928). Zur theorie des kristallwachstums. *Z. Phys. Chem.* **136**, 259-278.

Stranski, I. N. & Kaischew, R. (1934). Über den mechanismus des Gleichgewichtes kleiner kriställchen. I. *Z. Phys. Chem. B,* **26**, 100-113.

Swartzentruber, B. S. (1998). Fundamentals of surface step and island formation mechanisms. *J. Crystal Growth,* **188**, 1-10.

Swartzentruber, B. S., Mo, Y.-W., Kariotis, R., Lagally, M. G. & Webb, M. B. (1990). Direct determination

of step and kink energies of vicinal Si(001). *Phys. Rev. Letters,* **65**, 1913-1916.

Teng, H. H., Dove, P. M., Orme, C. A. & De Yoreo, J. J. (1998). Thermodynamics of calcite growth: baseline for understanding biomineral formation. *Science,* **282**, 724-727.

ten Wolde, P. R. & Frenkel, D. (1997). Enhancement of protein crystal nucleation by critical density fluctuations. *Science,* **277**, 1975-1978.

Theil, E. C. (1987). Ferritin: structure, gene regulation, and cellular function in animals, plants and microorganisms. *Annu. Rev. Biochem.* **56**, 289-315.

Thomas, B. R., Carter, D. & Rosenberger, F. (1997). Effects of microheterogeneity on horse spleen apoferritin crystallization. *J. Crystal Growth,* **187**, 499-510.

Van der Eerden, J. P. (1994). Crystal growth mechanisms. In *Handbook of Crystal Growth* (Hurle, D., ed.), vol. 1a, pp. 307-476, North Holland, Amsterdam.

Vekilov, P. G. & Rosenberger, F. (1996). Dependence of lysozyme growth kinetics on step sources and impurities. *J. Crystal Growth,* **158**, 540-551.

Vekilov, P. G., Monaco, L. A. & Rosenberger, F. (1995). Facet morphology response to non-uniformities in nutrient and impurity supply. I. Experiments and interpretation. *J. Crystal Growth,* **156**, 267-278.

Vekilov, P. G., Alexander, J. I. D. & Rosenberger, F. (1996). Nonlinear response of layer growth dynamics in the mixed kinetics-bulk transport regime. *Phys. Rev. E,* **54**, 6650-6660.

Vekilov, P. G., Thomas, B. R. & Rosenberger, F. (1998). Effects of convective solute and impurity transport on protein crystal growth. *J. Phys. Chem.* **102**, 5208-5216.

Volmer, M. (1939). *Kinetik der Phasenbildung*, Steinkopff, Dresden.

Warren, W. S. (1998). Rethinking solution NMR. *Science,* **280**, 398-399.

Weber, P. C. (1997). Overview of protein crystallization methods. In *Methods in Enzymology* (Carter, C. W., Jr & Sweet, R. M., eds), vol. 276, pp. 13-22, Academic Press, New York.

Weinkauf, S., Bacher, A., Baumeister, W., Ladenstein, R., Huber, R. & Bachmann, L. (1991). Correlation of metal decoration and topochemistry on protein surfaces. *J. Mol. Biol.* **221**, 637-645.

Williams, E. D. & Bartelt, N. C. (1991). Thermodynamics of surface morphology. *Science,* **251**, 393-400.

Wütrich, K. (1995). NMR: this other method for protein and nucleic acid structure determination. *Acta Crystallog. sect. D,* **51**, 249-270.

Yau, S.-T. & Vekilov, P. G. (2000). Visualization of nuclei structure and nucleation pathways. *Nature,* **406**, 494-497.

Yau, S. T., Thomas, B. R. & Vekilov, P. G. (2000). Molecular mechanisms of crystallization and defect formation. *Phys. Rev. Letters,* **85**, 353-356.

Yip, C. M. & Ward, M. D. (1996). Atomic force microscopy of insulin single crystals: direct visualization of molecules and crystal growth. *Biophysical J.* **71**, 1071-1078.

Yip, C. M., DePhelippis, M. R., Frank, B. H., Brader, M. L. & Ward, M. D. (1998). Structural and morphological characterization of ultralente insulin crystals by atomic force microscopy: evidence of hydrophobically driven assembly. *Biophysical J.* **75**, 1172-1179.

Edited by W. Baumeister

(Received 25 July 2000; received in revised form 5 September 2000; accepted 5 September 2000)